Oxidative dissolution of doped UO_2 and H_2O_2 reactivity towards oxide surfaces

A kinetic and mechanistic study

Kristina Nilsson

Licentiate Thesis

School of Chemical Science and Engineering,
Applied Physical Chemistry,
KTH Royal Institute of Technology
Sweden

Akademisk avhandling som med tillstånd av KTH i Stockholm framlägges till offentlig granskning för avläggande av teknisk licentiatexamen tisdagen den 10 juni kl. 10:00 i sal K2, Teknikringen 28, KTH, Stockholm.

TRITA-CHE Report 2014:23
ISSN: 1654-1081
ISBN: 978-91-7595-149-2

“Logic will get you from A to B,
imagination will get you everywhere”

Albert Einstein

Abstract

Oxidative dissolution of std. UO_2 and UO_2 doped with Cr_2O_3 and Al_2O_3, i.e. ADOPT, induced by H_2O_2 and γ radiation has been the main focus in this licentiate thesis. The catalytic decomposition of H_2O_2 on oxides like Gd_2O_3, HfO_2, CeO_2, Fe_2O_3 and CuO were also investigated.

A kinetic study was performed by determining first and second order rate constants together with Arrhenius parameters for the decomposition of H_2O_2. The reactivity of H_2O_2 towards the oxides mentioned was observed to differ significantly despite their similarities. In the mechanistic study, the yields and dynamics of the formation of the intermediate hydroxyl radical from the decomposition of H_2O_2 was determined for the oxides and found to differ considerably. A turnover point could be found for most of oxides studied, i.e. an increase in the rate of hydroxyl radical scavenging after a specific amount of consumed H_2O_2.

The reactivity of the std. UO_2 and ADOPT towards H_2O_2 was similar to what was observed for other UO_2-based materials in previous studies. The oxidative dissolution in radiation experiments showed a slight but significant difference. This was attributed to a difference in exposed surface area instead of an effect of doping. The difference in oxidative dissolution yield was too small to be significant which supports the previous conclusion.

Leaching experiments using spent nuclear fuel were also performed on the two types of fuel showing the same behavior as the unirradiated pellets, i.e., a slightly lower ^{238}U release from ADOPT. The difference was attributed to difference in exposed surface area. The release of fission products with low UO_2 solubility displayed a higher release from ADOPT which was attributed to a difference in matrix solubility. Cs was released to a larger extent from std. UO_2. This is attributed to the larger grain size of ADOPT, extending the diffusion distance. The release of lanthanides and actinides was slightly higher for the conventional UO_2, nevertheless the difference was relatively small.

Keywords

Oxidative dissolution; UO_2; ADOPT; H_2O_2; Spent Nuclear Fuel.

Sammanfattning

I det fall då kopparkapseln inneslutande utbränt kärnbränsle skulle gå sönder i ett slutförvar, och grundvatten kommer i kontakt med kärnbränslet bestående av främst UO_2, så kommer den strålningsinducerade upplösningen av UO_2 att resultera i en frisättning av radionuklider. Dessa processer är viktiga i säkerhetsanalysen av slutförvaret och flera modeller har utvecklats genom åren för att förutsäga upplösningshastigheter för UO_2 matrisen.

Oxidativ upplösning av std. UO_2 och UO_2 dopad med Cr_2O_3 och Al_2O_3, s.k. ADOPT, orsakad av H_2O_2 och andra radiolysprodukter av vatten har varit huvudfokus i denna licentiatuppsats. Den katalytiska sönderdelningen av H_2O_2 på oxider såsom Gd_2O_3, HfO_2, CeO_2, Fe_2O_3 och CuO undersöktes också.

En kinetisk studie utfördes genom att första och andra ordningens hastighetskonstanter och Arrhenius parametrar bestämdes experimentellt genom att följa sönderdelningen av H_2O_2. Man kan dra slutsatsen att reaktiviteten av H_2O_2 mot dessa oxider skiljer sig avsevärt trots likheterna mellan oxiderna. Mekanistiska studier har utförts där utbytet och dynamiken i bildandet av hydroxylradikalen från nedbrytning av H_2O_2 bestämdes för oxiderna. Även dessa utbyten skiljer sig avsevärt mellan oxiderna.

Reaktiviteten för std. UO_2 och ADOPT mot H_2O_2 är i samma storleksordning som i tidigare studier på UO_2-baserade material. Den oxidativa upplösningen i strålningsexperiment visade en liten men signifikant skillnad, vilket tillskrivs en skillnad i den exponerade ytarean snarare än en effekt av dopningen. Skillnaden i oxidativt upplösningsutbyte var för liten för att vara signifikant vilket leder till samma slutsats.

Lakningsförsök med använt kärnbränsle utfördes också på de två bränsletyperna. Resultaten visar på samma beteende som de obestrålade kutsarna, d.v.s. en något lägre ^{238}U frisättning från ADOPT. Skillnaden tillskrevs skillnaden i exponerad yta. Frisläppningen av fissionsprodukter med låg UO_2 löslighet visade en högre frisättning från ADOPT som tillskrevs

en skillnad i matrislösligheten. Cs frisläpptes i en större utsträckning från std. UO_2 vilket beror på den större kornstorleken hos ADOPT som resulterar i en förlängning av diffusionsavståndet. Frisättningen av lantanider och aktinider var något högre för std. UO_2 även om skillnaden var relativt liten.

List of Papers

Paper I

"Catalytic decomposition of hydrogen peroxide on transition metal and lanthanide oxides"

Cláudio M. Lousada, Miao Yang, Kristina Nilsson and Mats Jonsson.

Journal of Molecular Catalysis A: Chemical 379(2013) 178-184

Paper II

"Oxidative dissolution of ADOPT compared to standard UO_2 fuel"

Kristina Nilsson, Olivia Roth and Mats Jonsson. (To be submitted)

My contributions to the papers

I. I have performed part of the experiments and participated in the discussions and analysis of data.

II. I have participated in the planning, performed all experiments and written the manuscript.

Table of Contents

1. Introduction

In Sweden, two types of nuclear reactors are currently in operation, pressurized water reactor PWR and boiling water reactor BWR [1]. As a by-product to electricity production, these reactors are generating radioactive waste, mainly spent nuclear fuel. The spent nuclear fuel is proposed to be stored in a deep geological repository according to the KBS-3 concept schematically presented in Fig 1. The purpose of the repository is to completely isolate the spent nuclear fuel, during an assessment period of at least 100 000 years [2]. The spent nuclear fuel, containing ~5% fission products and actinides, will be kept in sealed cast iron canisters with an outer layer of copper. The canisters will be surrounded by bentonite clay. The repository will be located 500 meters below ground in the granitic bedrock. In the event of a canister failure accompanied by groundwater intrusion, the UO_2 matrix will be in contact with the groundwater and radionuclides can be released to the environment. The solubility of the matrix will govern the release of the major part of the radionuclides contained by the UO_2-matrix. However, the fraction of the radionuclides that have low solubility in the matrix are present at grain boundaries and are more readily dissolved upon contact with water, so called instant release. Understanding the dissolution behavior of UO_2 in water is of vital importance when assessing the safety of a final repository [3]. The main barriers of the repository are briefly summarized:

- Bedrock
    - Will isolate, provide mechanical stability and a stable chemical environment.
- Bentonite clay
    - Buffer material which will protect the canister from corrosive species and also protect the environment from radionuclides, in the event of a canister failure by acting as a diffusion barrier with high retention of cationic radionuclides.
    - Plastic properties of the clay will provide protection towards small movements in the bedrock.
- Copper canister/ cast iron
    - The outer copper part will provide corrosion resistance while the inner cast iron part will provide mechanical stability.

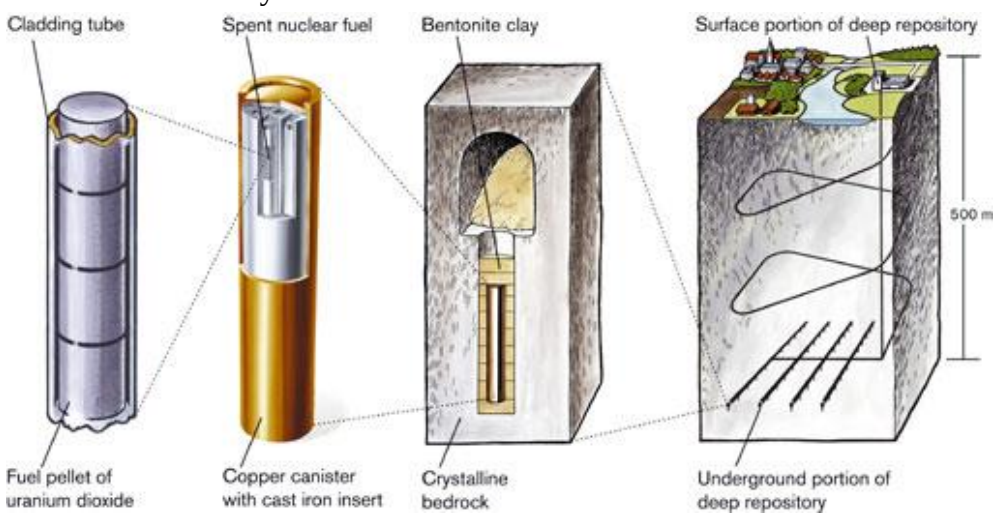

Figure 1. The KBS-3 concept for the Swedish deep repository for spent nuclear fuel [4].

The integrity of all the barriers has been thoroughly studied since the 1980's. The focus of this work is oxidative dissolution of the UO_2 matrix.

1.1 Properties of nuclear fuel before and after use

There are significant differences between fresh and spent nuclear fuel. The unirradiated nuclear fuel is composed of UO_2 while spent nuclear fuel also contains fission products and actinides as a result of the fission process. In the manufacturing of nuclear fuel, UO_2 is enriched from 0.7% to 3-5% of ^{235}U depending on where in the reactor it will be located [5]. The crystal structure of UO_2 is of fluorite (CaF_2) type as illustrated in Fig 2.

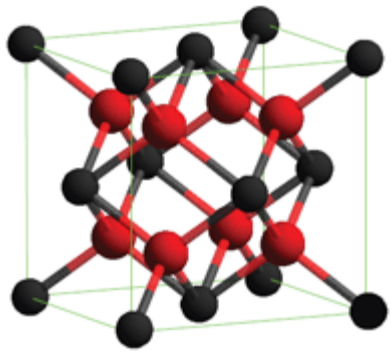

Figure 2. Crystal structure of UO_2 (U in black and O in red).

In recent years, new types of fuels with improved in-reactor performance have been developed. This calls for extended studies also of these materials for the safety assessment of future repositories. One of the new fuel types is ADOPT (Advanced Doped Pellet Technology). This type of fuel has been developed in order to reduce the fuel cycle cost and fuel failure and to improve flexibility and reliability of operation. It was first introduced for light water reactors (LWRs) in 1999 [6].

The ADOPT fuel is UO_2-based and doped with 1 000 ppm of chromium and aluminum oxides in total. The fuel was developed by Westinghouse Electric Sweden AB. The pellet has an increased density and enlarged grain size that has been shown to reduce the Fission Gas Release (FGR). Other advantages that have been shown

are the increased pellet cladding interaction margins and the improved resistance to post failure degradation [6]. The enlarged grain size implies a longer diffusion path and thereby gaseous fission products are retained in the matrix [6, 7].

The properties of Spent Nuclear Fuel (SNF) depend on the fuel fabrication (enrichment of ^{235}U), burnup and operational parameters for the in-reactor use. In general, in-reactor use of the nuclear fuel will induce chemical changes as well as changes in the microstructure. While the fresh nuclear fuel is a very homogeneous material, the spent nuclear fuel is very heterogeneous both in terms of chemical composition and microstructure. Increasing the burnup has been a trend during recent years and research has been focused on the rapid release fractions of fission products from high burnup fuel [8]. Fuel with high burnup will have an even more significantly transformed microstructure in the outer region of the pellet compared to fuel with more conventional burnup. This feature is also known as high burnup structure or rim structure. The microstructure of high burnup fuel consists of small grains of submicron size and the concentration of pores (with a diameter of 1-2 μm) is high. These structural changes occur in UO_2 fuel when the local burnup exceeds 50 MWd/kgU, provided that the temperature has not exceeded 1000–1100°C. The structural changes in the periphery of the pellet are due to the buildup of plutonium by the neutron capture in ^{238}U, with the consequence of fission of the formed plutonium [8, 9].

As can be understood from the obvious differences between fresh and spent fuel, the reactivity of spent nuclear fuel is not expected to be identical to the reactivity of pure UO_2. From a purely chemical point of view, spent nuclear fuel can be regarded as doped UO_2 [10, 11]. Hence, studies on pure UO_2 may not be directly applicable when trying to understand the behavior of spent nuclear fuel under deep repository conditions. Nevertheless, UO_2 is the main constituent also of spent nuclear fuel and understanding the properties of pure UO_2 is

essential for the understanding of the more complex material of relevance in the safety case. In addition to studies on pure UO_2, studies on UO_2 doped with various elements to mimic the incorporation of fission products or to increase the radioactivity of the matrix are also important.

A way to circumvent the obvious difficulties connected to experimental studies of spent nuclear fuel is to study model materials with some features in common with spent nuclear fuel. One of the most commonly studied model materials is SIMFUEL, which consists of UO_2 doped with non-radioactive isotopes of Ba, Ce, La, Mo, Sr, Y, Zr, Pd, Rh, Ru and Nd mimicing the chemical changes (inclusion of fission products) induced by in-reactor exposure [12]. The dopants can be divided into different groups depending on their solubility in UO_2. Trivalent rare earth elements (RE^{3+}) are acting like dopants in the U(IV) oxide structure and due to their presence there, the electrical conductivity is increased. Dopants like Pd, Ru and Rh and Mo will segregate and form noble-metal alloy particles called ε-particles due to their instability in the oxide matrix [12, 13].

1.2 Dissolution of spent nuclear fuel

In the event of canister failure and intrusion of groundwater, radionuclides can be released from the spent nuclear fuel. The release occurs through two different processes, instant release and matrix dissolution. The Instant Release refers to the release of volatile and segregated fission products, Fig. 3, that are present in the gap between the fuel and the cladding or in the grain boundaries. The Instant Release Fraction (IRF) is an important parameter when assessing the safety of geological repositories [14, 15].

Radionuclides of low matrix solubility are enriched at the grain boundaries and are expected to be released more rapidly as illustrated in Fig. 3. Actinides and lanthanides soluble in the UO_2 matrix are expected to follow the dissolution of the UO_2 matrix [12].

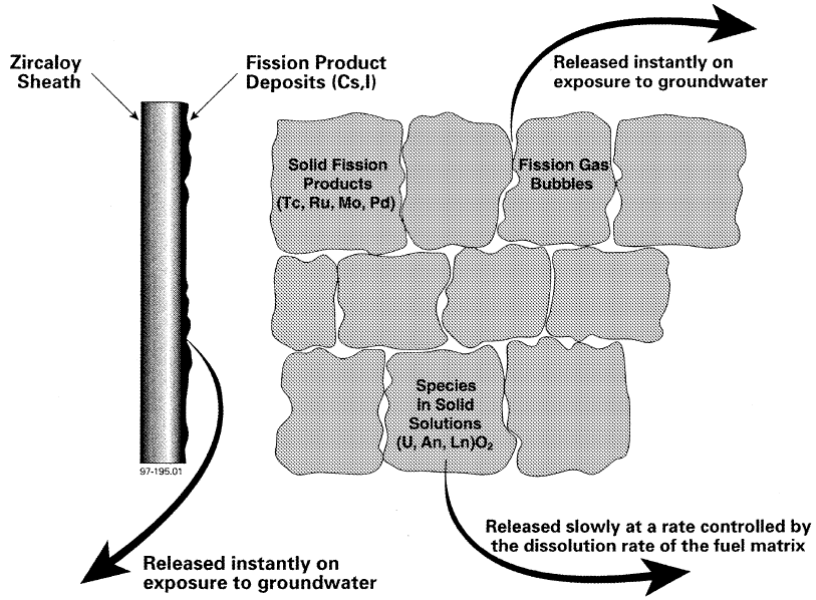

Figure 3. The distribution of radionuclides in used fuel [12].

Matrix dissolution can occur through two different processes; (1) dissolution of the UO_2 and (2) oxidative dissolution. The UO_2 matrix has low solubility under reducing conditions and these are the conditions expected to prevail at repository depth. However, the redox conditions will change due to radiolysis of the groundwater producing oxidants that can oxidize the UO_2 surface to U(VI) and thereby increase the matrix solubility [12, 16]. The presence of complexing agents such as HCO_3^- will enhance the solubility further due to formation of highly soluble carbonate complexes with U(VI). In the presence of HCO_3^-, the rate limiting step is oxidation [17].

The overall oxidative dissolution of UO_2 can be viewed below where the first step, Reaction 1, involves the oxidation of the surfaces bound UO_2 and the second step, Reaction 2, is the subsequent dissolution of oxidized UO_2(s).

$$UO_2 + OX \rightarrow UO_2^{2+}(s) + RED \quad (1)$$

$$UO_2^{2+}(s) \rightarrow UO_2^{2+}(aq) \quad (2)$$

Oxidation can be achieved by both one- and two-electron oxidants:

One-electron oxidants

$$UO_{2(surf)} + 1\text{-}e^{-}OX \rightarrow UO_2^{+}{}_{(surf)} + 1\text{-}e^{-}\ RED \qquad (3)$$

$$UO_2^{+}{}_{(surf)} + UO_2^{+}{}_{(surf)} \rightarrow UO_{2(surf)} + UO_2^{2+}{}_{(surf)} \qquad (4)$$

$$UO_2^{+}{}_{(surf)} + 1\text{-}e^{-}OX \rightarrow + UO_2^{2+}{}_{(surf)} + 1\text{-}e^{-}\ RED \qquad (5)$$

Two-electron oxidants

$$UO_{2(surf)} + 2\text{-}e^{-}OX \rightarrow UO_2^{2+}{}_{(surf)} + 2\text{-}e^{-}\ RED \qquad (6)$$

1.3 Radiation chemistry and radiolysis of water

Ionizing radiation (high energy particles and photons) interacts with matter mainly through interactions with the electrons of the absorber. The main exception from this is neutron radiation which involves interaction with nuclei of the absorber and thereby the possibility of inducing radioactivity. Upon absorption of ionizing radiation, the absorbing material is ionized and electronically excited. Consequently, the absorption process will induce chemical changes in the absorber. These chemical changes constitute the basis of radiation chemistry. To quantify the chemical changes induced by ionizing radiation, the absorbed dose (i.e. the absorbed radiation energy) must be known in combination with the efficiency in converting radiation energy to chemical change. The latter is referred to as the radiation chemical yield or the G-value. This entity depends on the absorbing material and the type and energy of the radiation and has the unit mol J^{-1}. The absorbed dose, D, has the SI unit 1 Gy (J kg^{-1}). The dose rate describes the rate of absorbed dose per unit time, $\dot{D}$, given in Gy s^{-1} [5].

Water exposed to ionizing radiation will undergo radiolysis according to Reaction 7 [18]. The primary processes in water radiolysis are

illustrated in Fig. 4**.** The series of events can be divided into three main stages. The *physical stage* includes the initial matter ionizing radiation interaction, leading to the formation of ionized water molecules (H_2O^+), excited water molecules (H_2O^*) and sub-excitations electrons (e^-). The *physico- chemical stage* includes processes like Ion-molecule reaction (8), Dissociative relaxation (9) and solvation of electrons (10). The last step called the *chemical stage* involves the created species before will now react with each other or with surrounding molecules in the tracks and diffuse in the solution.

$$H_2O \xrightarrow{\text{Ionizing Radiation}} e_{aq}^-, HO^\cdot, H^\cdot, HO_2^\cdot, H_3O^+, OH^-, H_2O_2, H_2 \quad (7)$$

$$H_2O^+ + H_2O \rightarrow H_3O^+ + HO^\cdot \quad (8)$$

$$H_2O^* \rightarrow HO^\cdot + H^\cdot \quad (9)$$

$$e^- \rightarrow e_{aq}^- \quad (10)$$

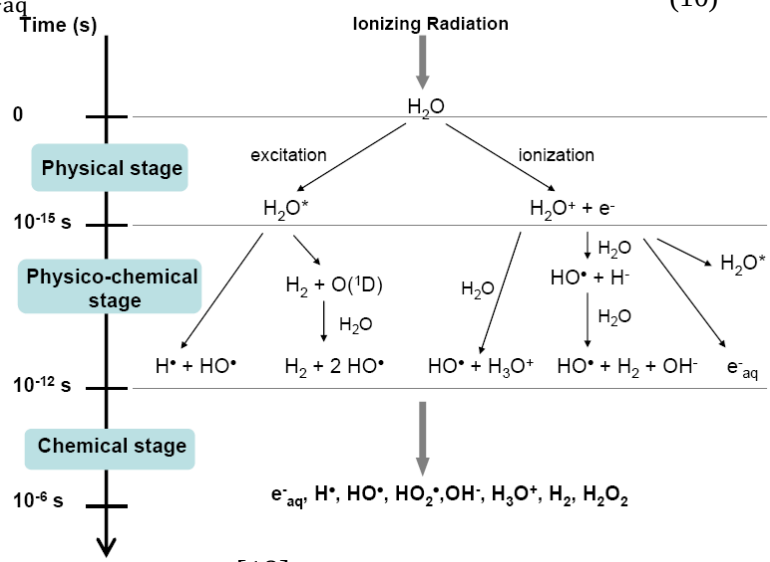

Figure 4. Radiolysis of water [18].

The radiation chemical yields for radiolysis of water are presented in table 1 [13].

Table 1. G-values for radiolysis products (μmol J^{-1}) [5].

	$G(H_2O)$	$G(e_{aq}^-)$	$G(HO^\cdot)$	$G(H^\cdot)$	$G(HO_2^\cdot)$	$G(H_2O_2)$	$G(H_2)$
γ and fast electrons	-0.43	0.28	0.28	0.062	0.0027	0.073	0.047
12 MeV He^{2+}	-0.2974	0.0044	0.056	0.028	0.007	0.112	0.115

1.4 Surface chemistry and reactivity

Surface reactions such as the oxidative dissolution of spent nuclear fuel can generally be illustrated by Fig. 5. The solute reactant will diffuse to the surface where it is adsorbed. The subsequent surface reaction proceeds via one or several transition states and the final product desorbs from the surface and diffuses into solution. Every step of the process can be related to a rate constant. However, in practice it is very difficult to determine these rate constants individually.

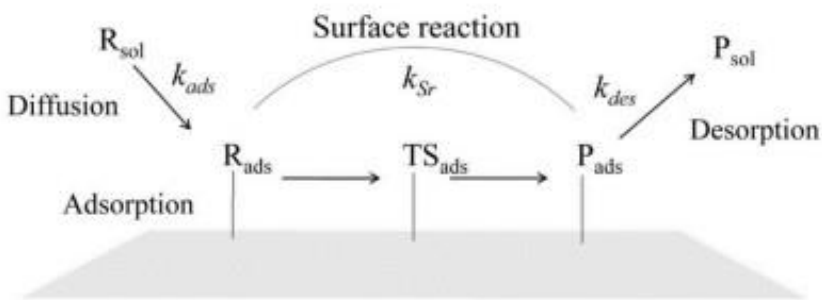

Figure 5. The steps involved in a surface reaction [19].

The surface structure is of key-importance for the energetics and kinetics of surface reactions. There is a variety of surface topology features present at surfaces as seen in Fig. 6. These features have different surface energies. As an example, dissolution of CaF_2 in contact with 0.05 M $NaClO_4$ was investigated by J.R.A Godinho *et al* [20]. Interestingly, the dissolution rates were found to depend on

surface orientation, with more or less stable planes, and surface topography. A correlation between dissolution rate and the density of steps between reference planes was observed.

The incorporation of dopants in a material can change the surface structure, as can be seen in the case of UO_2 doped with Cr_2O_3 and Al_2O_3 oxides as mentioned earlier.

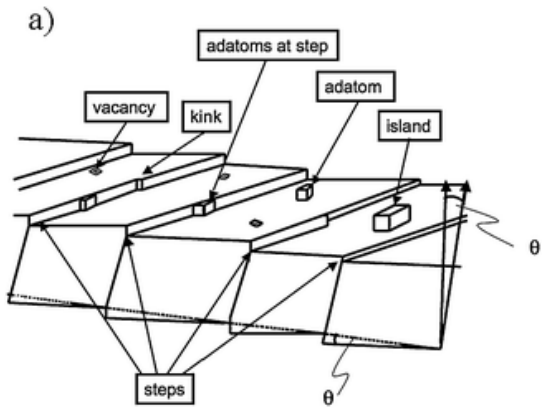

Figure 6. Sites on the surface with different energies [21].

Both Cr_2O_3 [6, 7] and Al_2O_3 [22] have been found to increase the grain size. Earlier studies of different additives have been performed; Cr_2O_3 [23-26], Al_2O_3 [22] and Nb_2O_3 [7]. Fabricated fuel is slightly hyper-stoichiometric UO_{2+x}($x \leq 0{,}001$) [12]. The stoichiometric UO_2 has a smooth surface with featureless grains, while the hyper-stoichiometric surface have characteristic facetted or/and ridged structures [27]. The hyper-stochiometry will be reduced during the formation of $CrUO_4$ due to the removal of excess oxygen from the UO_{2+x} lattice. This will result in an altered stability of the fission products in solution, as they are more stable in UO_{2+x} than UO_2. Al_2O_3 was shown to be soluble in $CrUO_4$, forming $(Cr,Al)UO_4$, but $AlUO_4$ could not be formed [26]. This could suggest that a Cr/Al doped UO_2 should have a smother surface, i.e. less features like ridges or /and facetted structures.

1.5 Radiation induced oxidative dissolution of UO_2

Aqueous radiolysis of groundwater in contact with spent nuclear fuel will produce both oxidants and reductants. For kinetic reasons, the radiolytic oxidants will dictate the surface chemistry of the fuel matrix, at least initially. The primary oxidants produced upon radiolysis of pure water are H_2O_2 and $OH^{\bullet}$. However, as will be discussed below, in groundwater containing HCO_3^-, $OH^{\bullet}$ will rapidly be converted to $CO_3^{\bullet-}$. Among the aqueous radiolysis products, H_2O_2 is a two-electron oxidant while the hydroxyl radical, $HO^{\cdot}$, and the carbonate radical anion are one-electron oxidants. As illustrated by reaction 3-5, two one-electron oxidants are required to oxidize U(IV) to the more readily soluble U(VI). It was shown by M. Jonsson et al. [28] that the dissolution yield was higher for a two-electron oxidant, then for a one-electron oxidant. This was attributed to the lower probability of a second oxidation, especially in the case when the one-electron oxidant is present in low concentration.

The kinetics of UO_2 oxidation by radiolytic oxidants in water has been studied quite extensively and rate constants for all the relevant oxidants have been reported [29]. To be able to predict the dynamics of radiation induced oxidative dissolution of spent nuclear fuel, numerical simulation of the radiation chemistry of water must be employed taking into account all the relevant surface reactions. This is a fairly complicated procedure and efforts have been made to simplify without significantly reducing the accuracy of the predictive modeling [13, 30]. In a study by Ekeroth et al., the relative impact of aqueous radiolytic oxidants on radiation induced dissolution of UO_2 was studied [31]. The study was based on numerical simulations benchmarked with experimental data. On the basis of the kinetics of the individual reactions, it was concluded that the most important oxidant under a variety of different conditions is H_2O_2. However, it should be noted that this assessment was strictly based on the reactivity of UO_2 in the form of powder [31].

1.5.1 Reactivity of H_2O_2 towards UO_2

There are two different mechanisms by which H_2O_2 can react with UO_2: (1) oxidation of U(IV) to U(VI) leading to a dissolution of the matrix as seen in Reaction 11 and (2) catalytic decomposition of H_2O_2 according to Reaction 12 [32].

$$H_2O_2 + UO_2 \rightarrow 2HO^- + UO_2^{2+} \quad (11)$$

$$H_2O_2 \xrightarrow{UO_2} 2H_2O + \frac{1}{2}O_2 \quad (12)$$

Reaction 11 can be described more in detail as a fenton-like two-step process, reaction 13-14, with the first step reaction 13 being rate determining [33, 34].

$$H_2O_2 + UO_2 \rightarrow HO^{\cdot} + HO^- + UO_2^{+} \quad (13)$$

$$HO^{\cdot} + UO_2^{+} \rightarrow HO^- + UO_2^{2+} \quad (14)$$

The mechanism of the catalytic decomposition of H_2O_2 on an oxide surface is depicted below [35]. This mechanism was confirmed experimentally quite recently.

$$H_2O_2 + M \rightarrow 2HO^{\cdot} + M \quad (15)$$

$$HO^{\cdot} + H_2O_2 \rightarrow HO_2^{\cdot} + H_2O \quad (16)$$

$$2HO_2^{\cdot} \rightarrow H_2O_2 + O_2 \quad (17)$$

The competition between the two reactions consuming H_2O_2 is quite important in the assessment of the overall dissolution process. One way to quantify the competition has been to define a dissolution yield. The dissolution yield is simply the ratio between the dissolved U(VI) and consumed H_2O_2. In early studies on UO_2 powder suspensions, the dissolution yield was found to be around 80 % and the oxidation reaction was assumed to be the dominating reaction. However, as

studies were performed also on pellets and pellets doped with rare earth elements, it was concluded that the catalytic decomposition of H_2O_2 is in fact the dominating process for UO_2 based materials of relevance in spent nuclear fuel dissolution. The dissolution yields for some UO_2 based materials are presented in Table 2.

Table 2. Dissolution yields expressed as % of [U(VI)] in solution per [H_2O_2] consumed for different UO_2 based materials.

Material	Dissolution yield (%)
UO_2 powder	80 [28]
UO_2 pellet (Westinghouse)	14 [32]
SIMFUEL pellet	0.2 [32]
UO_2 pellet (in house)	6 [36]
UO_2/Y_2O_3 pellet (in house)	2.5 [36]
UO_2/Y_2O_3/Pd pellet (in house)	0.9 [29]
UO_2/Pd pellet (in house)	11.5 [37]

The reactivity of H_2O_2 towards other oxides has been studied quite extensively over the last years. The results from these studies are applicable for the understanding of the spent nuclear fuel dissolution. The adsorption of H_2O_2 onto the surface of metal oxides, as ZrO_2, TiO_2 and Y_2O_3, has been studied [38] both experimentally and theoretically, and two types of interactions could be seen; (i) The direct interactions between the O- atoms of H_2O_2 and metal atom being exposed on the surface (ii) Hydrogen bonding between the H_2O_2 and the OH groups on the surface.

There is a difference in the strength of adsorption through these two interactions. The first type of interaction results in stronger adsorption. Both types of interactions will occur, and ratio between

them will depend on the density of OH groups (depending on Lewis acidity).

The hydroxyl radical is the primary product of H_2O_2 decomposition for the oxide mentioned. The hydroxyl radical adsorbs to the surface through the formation of bonded states with the exposed metal atoms. The strength of adsorption, adsorption energy, was found to depend on the ionization energy of the metal cation. Higher ionization energy would result in a weaker adsorption of the hydroxyl radical.

1.5.2 Hydrogen inhibition of oxidative dissolution of spent nuclear fuel

Considerable amount of H_2 is expected to be produced due to the anaerobic corrosion of iron from the cast iron surrounding the fuel inside the canister in the event of a canister failure. H_2 is also produced during radiolysis of water. Hydrogen has been shown to inhibit the oxidative dissolution of spent nuclear fuel in numerous spent fuel leaching experiments. The rationale for this has been discussed for quite some time. Several mechanisms have been proposed but the only process that can fully account for complete inhibition is reduction of surface bound U(VI) catalyzed by noble metal inclusions (illustrated in fig. 5). The possible mechanisms have been discussed and compared [39]. In addition to the reduction of surface bound U(VI), the noble metal inclusions also catalyze the reaction between H_2O_2 and H_2. The presence of H_2 will also influence the radiolytic production of H_2O_2 in solution and reduce the oxidant concentration.

1.6 Effects of groundwater chemistry

The solubility of U(VI) is at a minimum in the pH range 7-10, and this happens to be the pH range of most repository ground waters. The dissolved UO_2^{2+} is likely going to be redeposited due to the low solubility. This will be the case, unless there is a significant HCO_3^-/CO_3^{2-} concentration present in the groundwater. HCO_3^- is a

complexing agent that will enhance the dissolution trough formation of soluble complexes with uranyl. This will result in an increased release of UO_2^{2+} from the surface to the solution. The consequent increase in solubility will thereby prevent redeposition of UO_2^{2+} and accelerate the oxidative dissolution kinetics [12, 13, 16].

$$UO_2^{2+} + aHCO_3^- \rightarrow UO_2(HCO_3)_a^{2-a} \qquad (18)$$

The radiolytically produced hydroxyl radical, $OH^{\cdot}$, can be scavenged by HCO_3^- according to Reaction 19 [39]. The reactivity of the carbonate radical anion towards UO_2 has been estimated to be the same as the reactivity of the hydroxyl radical [31].

$$OH^{\cdot} + HCO_3^- \rightarrow H_2O + CO_3^{\cdot -} \qquad (19)$$

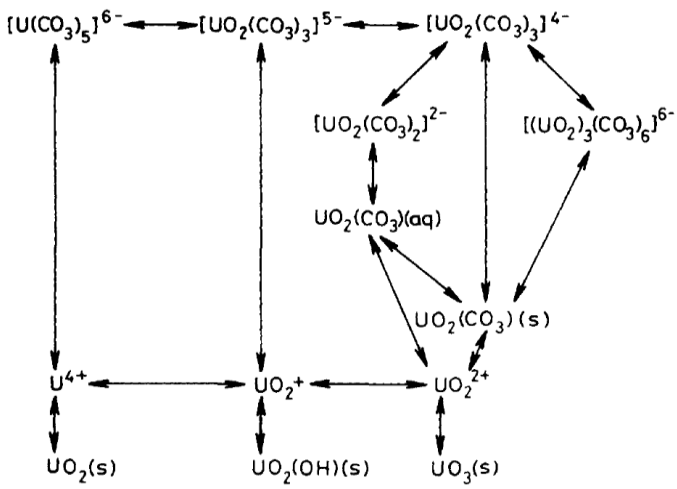

Figure 7. Thermodynamic cycle for the uranium (IV,V,VI)-water carbonate systems [16].

The second order rate constant for oxidation of UO_2 by H_2O_2 depends on the concentration of HCO_3^- below 1mM. The kinetics will depend on both oxidation and dissolution below this concentration. The kinetics of oxidative dissolution is thereby completely governed by the matrix oxidation process at concentrations above 1 mM HCO_3^-. Hence, it is of importance to have a concentration above 1 mM when

determining rate constants for oxidation of UO_2 by H_2O_2 [34]. The HCO_3^- concentration in granitic groundwater is 2-10 mM in Sweden [17]. The speciation is illustrated in Fig. 7.

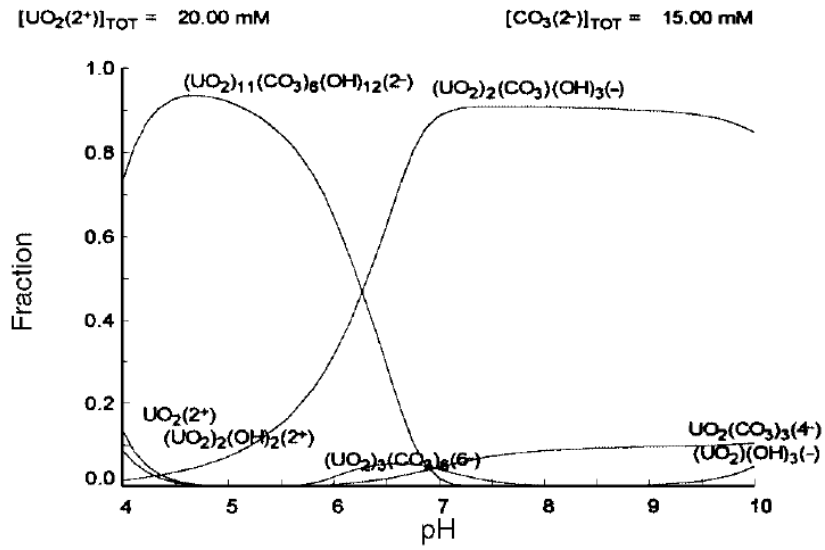

Figure 8. Uranium distribution diagram for the uranium(VI)-carbonate systems as a function of pH [40].

The main reactions involved in radiation induced dissolution and H_2 inhibition of the same process are illustrated in Fig. 9.

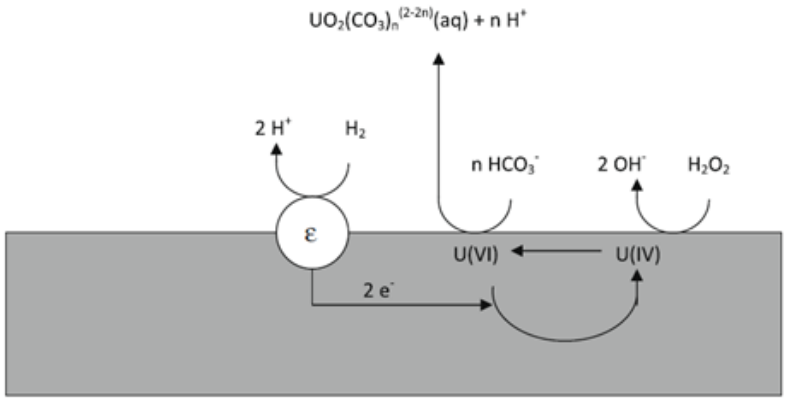

Figure 9. Elementary processes involved in radiation induced oxidative dissolution of UO_2 [39].

1.7 Aim of the study

The aim of the work presented in thesis is to enhance the understanding of the oxidative dissolution of UO_2.

This was done by;

- Investigating how the catalytic decomposition of H_2O_2 varies for different oxides.

- Investigating how the oxidative dissolution of UO_2 will change when the matrix is doped with Cr_2O_3 and Al_2O_3 oxides i.e. the ADOPT. This was done for both fresh pellets and spent fuel.

2. Experimental part

2.1 Materials and Equipment

The ADOPT and UO_2 pellets were supplied by Westinghouse AB. The oxides were provided by Alfa Aesar and Aldrich while the other chemicals were delivered from Merck, AGA and Air Liquid. Only Milli-Q filtered water (18 $M\Omega cm^{-1}$) was used throughout and the experiments were performed at room temperature, if not mentioned otherwise.

A ^{137}Cs γ-source with a dose rate depending on position. The dose rate in the central position is 0.15 Gy s^{-1}measured with Fricke dosimetry [5] (MDS Nordion Gammacell 1000 Elite) was used.

For UV/vis spectroscopy studies WPA Lightwave S2000 or a WPA Biowave II UV/Vis Spectrophotometer are used.

ICP-OES (Inductively Coupled Plasma-Optical Emission Spectrometry) was used for detecting Cr and Al present in solution.

BET equipment, Micromeritics flowsorb II 2300 with 30% N_2 in Helium, was used to obtain the specific surface area for the oxides studied.

2.2. Methods

2.2.1 The Arsenazo III method for U(VI) [II]

Determination of the uranyl UO_2^{2+} concentration was done using the Reagent Arsenazo III method [41]. 40 µL of Arsenazo III solution (0.3% Arsenazo III in 10% acetic acid) and 65 µL 1 M HCl are added to the cuvette, together with 1.5 ml from the sample solution. The sample solution consists of 10 mM $NaHCO_3$. The amount taken from the sample solution depends on concentration, and has to be diluted with water if the concentration is too high. The uranyl will form a complex with the Arsenazo III when reacting with the arsenic and azo group seen in Fig. 10. The absorbance is measured at the wavelength of 652 nm with UV/VIS spectroscopy.

Formation of U(VI) was measured at room temperature for the fresh std. UO_2 and the ADOPT pellet in paper [II].

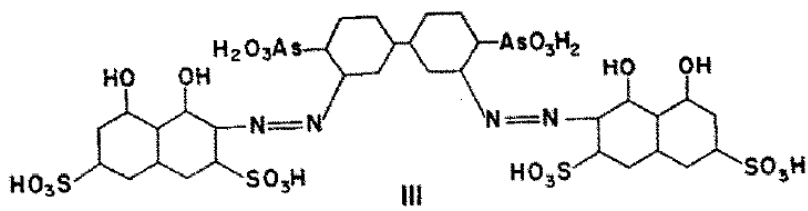

Figure 10. The Arsenazo III [41].

2.2.2 Ghormley triiodide method for H_2O_2 [I] [II]

The concentration of H_2O_2 was determined using the Ghormley triiodide method [42], where H_2O_2 oxidizes I^- to I_3^-, as seen in Reaction 20 and 21. The absorbance of I_3^- is then measured at the wavelength of 360nm with UV/VIS spectroscopy.

$$H_2O_2 + 2H^+ + 2I^- \rightarrow 2H_2O + I_2 \qquad (20)$$

$$I_2 + I^- \rightarrow I_3^- \qquad (21)$$

100 µl 1 M KI and 100 µl 1 M $NaOOCCH_3$/ 1 M CH_3CO_2H are added to a cuvette. The amount of the sample solution depends on the start concentration of H_2O_2 and is added before the MQ water. The amount of the MQ water is adjusted to have a total volume of 2 ml.

The sample solution has to be filtered in the case of using powders as in paper [I]. The consumption of H_2O_2 was obtained for the oxides Gd_2O_3, HfO_2, CeO_2, Fe_2O_3 and CuO as powders at different temperatures (25, 40, 60 and 75℃) and at room temperature for the std. UO_2 and ADOPT pellet in paper [II].

2.2.3 The modified version of Hantzsch method for detection of HO˙ [I]

The concentration of $OH^{\cdot}$ was determined by measuring the concentration of formaldehyde at 368 nm with UV/VIS spectroscopy according to the modified version of Hantzsch method [35]. Formaldehyde H_2CO is formed in a reaction between $OH^{\cdot}$ and tris(hydroxymethyl)aminomethane as seen in Fig. 11, in the reaction solution. Formaldehyde is then quantified in a test tube at 40℃ after reacting with acetoacetanilide, AAA, in the presence of ammonium acetate, seen in Fig. 12. This will lead to the formation of a dihydropyridine derivative which is then detected with UV/vis at 368 nm.

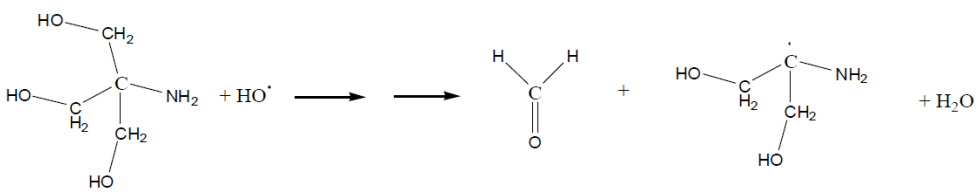

Figure 11. Tris and $OH^{\cdot}$ forming H_2CO.

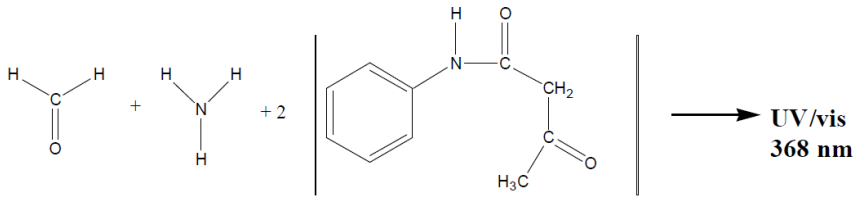

Figure 12. The formation of a dihydropyridine derivative.

pH of the Tris solution is first adjusted to pH 7.5 using HCl. 0.25 ml of 0.1M H_2O_2 is then added to 49.75 ml of the pH adjusted Tris. The sample bottle is placed in water bath to obtain the right temperature before the oxide can be added and the experiment can be started. The blank is taken just before adding the oxide and samples are subsequently taken during the experiment. The sample is stirred using a syringe with nitrogen gas and a lid has to cover the sample holder at temperatures above 60 degrees. For each sample; 1.5 ml solution is taken, filtered and added to a test tube together with 1 ml 0.2 M acetoacetanilide in ethanol and 2.5 ml of 4 M ammonium acetate solution and stored for 15 minutes at 40 °C and thereafter measuring the absorbance at 368 nm with UV/VIS spectroscopy as mentioned above. The formation of $HO^{\cdot}$ was determined for the oxides Gd_2O_3, HfO_2, CeO_2, Fe_2O_3 and CuO as powders in paper [I].

2.2.4. Leaching of spent fuel [II]

The fuel rods were irradiated in Oskarshamn 3 during 2000-08-10 to 2008-10-02. The standard fuel had an initial enrichment of 3.5 wt% U^{235}, rod average burn-up 57.1 MWd/kgU and a fission gas release of ~ 2.5 %. The ADOPT fuel had initial enrichment of 4.1 wt% U^{235}, rod average burn-up 59.1 MWd/kgU and a fission gas release of ~ 1.4 %.

The samples were prepared by cutting ~20 mm long pieces of each rod. The cladding of the rod segments were afterwards cut longitudinally by sawing on opposite sides of the segment. Force was

applied to the halves until the fuel broke away from the cladding. The two cladding halves, together with detached fuel fragments were weighed, collected in a glass vessel with glass filter bottom (100-160 µm pores) and immersed into 200 ml leaching solution (10 mM NaCl + 2 mM $NaHCO_3$).

The leaching experiments were performed using samples from two high burnup fuels (one standard UO_2 fuel and one ADOPT fuel) provided by Westinghouse AB. The leaching was performed in air in batch experiments divided in contact periods. After each contact period the fuel sample was transferred to a new flask containing fresh leaching solution.

From the used leaching solution, samples were collected for ICP-MS (Inductively Coupled Plasma-Mass Spectrometry) isotopic and γ-spectrometric analyses, as well as for pH and carbonate determination (pH and carbonate results were fairly constant during all the tests). Details on analyses and corrections (e.g. isobaric interferences) that are applied to the raw ICP-MS data can be found in Zwicky et al. [9]. The contact periods were 1, 7, 23, 56, 91 and 182 days. The experiments has previously been described in [14, 15].

Release fractions for the radionuclides describe the amount of each nuclide measured from the leachant divided by the initial the amount of the nuclide in the fuel sample. Cumulative release fractions are then obtained when adding the release fractions from each contact period. Fractional release rates are obtained by dividing the release fractions by the length of the contact period.

3. Results and Discussion

3.1 Catalytic decomposition of hydrogen peroxide on transition metal and lanthanide oxides

The aim in paper I was to enhance the understanding of catalytic decomposition of H_2O_2 on oxides that cannot be oxidized. This was done in order to later be able to draw conclusions for the UO_2 system.

The reactivity of H_2O_2 towards the different oxides used in this study e.g. Gd_2O_3, HfO_2, CeO_2, Fe_2O_3 and CuO has been examined [43]. It was revealed that there is a significant difference when it comes to energetic and kinetic parameters.

The catalytic decomposition of H_2O_2 is illustrated in Fig. 13, where the normalized concentration of H_2O_2 is followed as a function of reaction time. It can be seen from the shape of the curves for some of the oxides that there is a faster initial consumption of H_2O_2 which is attributed to its adsorption to the surface followed by slower consumption which follows first order kinetics. This is mainly seen for CeO_2 and Gd_2O_3 which means that the kinetic data collected for them only fits first order kinetics within a limited H_2O_2 concentration range. For both CuO and HfO_2, the reaction follows first order behavior during the whole reaction time.

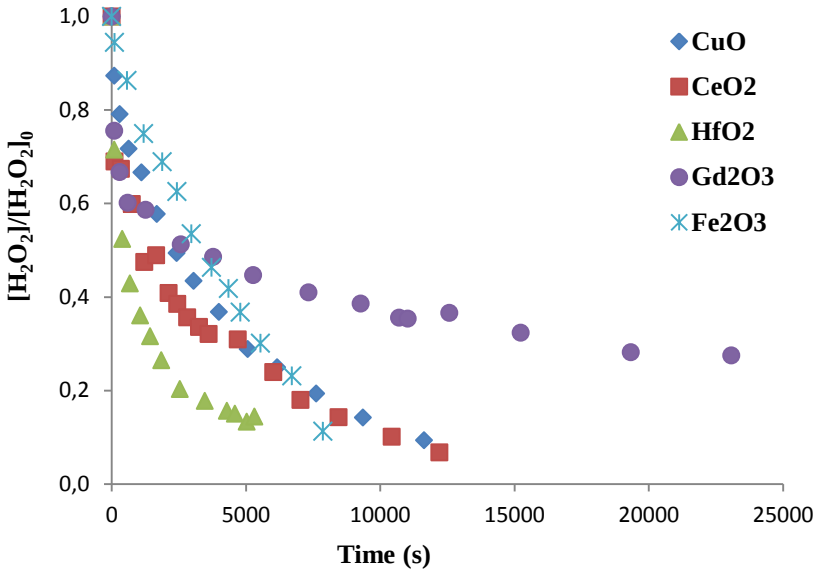

Figure 13. Normalized concentration of H_2O_2(initially 0.5 mM in 50 ml) as a function of reaction time for the reaction with CeO_2(red square), CuO (blue diamond), HfO_2 (green triangle), Gd_2O_3(purple circle) and Fe_2O_3(blue stars) at T = 298.15 K. SA: Fe_2O_3(4.5 m^2), CeO_2(7.5 m^2); CuO (0.3 m^2); HfO_2(7.5 m^2);Gd_2O_3(1.7 m^2)

The second-order rate constants, k_2, are obtained from Fig. 14 and viewed in Table 3, where the first order rate constants are plotted as a function of solid surface area to solution volume ratio S_A/V according to equation 22;

$$\frac{-d[A]}{dt} = k_2 \left(\frac{SA_{oxide}}{V}\right)[A] \qquad (22)$$

Where SA_{oxide} is the surface area of the powder, V the volume of the reactant solution and k_2 is the second order rate constant. Different surface area to solution ratios were obtained by using different amounts of each powders, while keeping the volume of the solution constant. The particle size of the powders was measured by BET.

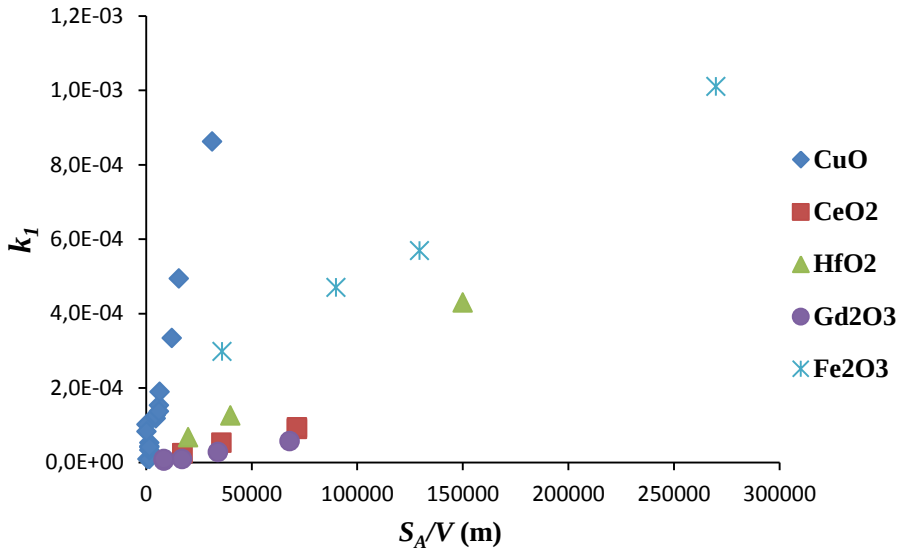

Figure 14. Variation in first-order rate constant (k1) with the surface-area-to-solution-volume-ratio (SA/V) of oxide for decomposition of H_2O_2 (0.5 mM; 50 ml) at T = 298.15 K. CeO_2 (red square), CuO (blue diamond), HfO_2 (green triangle), Gd_2O_3(purple circle) and Fe_2O_3(blue stars).

Table 3. The first order (k_1) and second order (k_2) rate constants and the intercept at the zero coordinate (b_2).

Material	k_1 (s^{-1})[a]	k_2 ($m \cdot s^{-1}$)	b_2 (s^{-1})
Fe_2O_3	$(2.1 \pm 0.4) \times 10^{-4}$	$(3.0 \pm 0.06) \times 10^{-9}$	2×10^{-4}
CeO_2	$(1.7 \pm 0.5) \times 10^{-4}$	$(2.80 \pm 0.07) \times 10^{-8}$	5×10^{-6}
CuO	$(1.90 \pm 0.05) \times 10^{-4}$	$(1.23 \pm 0.06) \times 10^{-9}$	6×10^{-6}
HfO_2	$(4.3 \pm 0.9) \times 10^{-4}$	$(2.78 \pm 0.02) \times 10^{-9}$	1×10^{-5}
Gd_2O_3	$(3.6\pm 0.3) \times 10^{-5}$	$(9.4 \pm 1) \times 10^{-10}$	6×10^{-6}

[a] conditions according fig.12

3.1.1 Arrhenius parameters

The temperature dependence of the catalytic decomposition of H_2O_2 on the oxides mentioned was used to determine the Arrhenius parameters, the activation energy E_a and the frequency factor A. The logarithm of the first order rate constants (k_1) was plotted as a function of the inverse absolute temperature ($^1/_T$). The activation energy was gained from the slope in Fig. 15 while the frequency factor was taken from the intercept according to equation 23 and 24,

$$k_1 = Ae^{-\frac{E_a}{RT}} \quad (23)$$

$$ln\, k_1 = ln\, A\, - \frac{E_a}{R} \quad (24)$$

Where $k_1$is the reaction rate constant, A is frequency factor, E_a is the activation energy, R is the gas constant and T is the absolute temperature. The values of the activation energy, frequency factor and the particle size for each oxide can be found in table 4. There is a significant variation in the E_a for the oxide studied. The lack of correlation between E_a and the oxide stoichiometry could indicate that the E_a is dependent on the type of atom at the active site and the degree of hydroxylation. Most oxides exposed to water will get a hydroxylated surface, due to the dissociative adsorption of H_2O [44]. The degree of hydroxylation will depend on the extent of Lewis acidity. The Lewis acidity is related to the Ionization Potential which has been seen to correlate to the E_a [19], which will be discussed more in the next section.

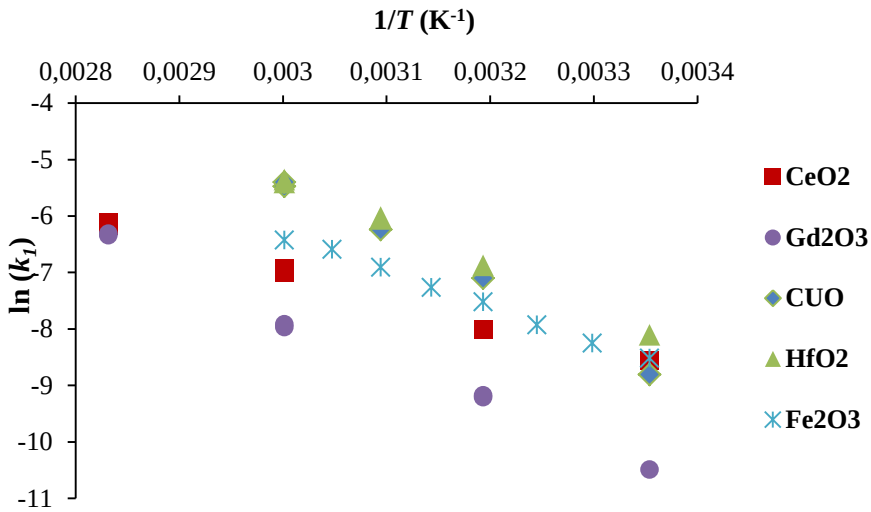

Figure 15. Arrhenius plots for the first-order rate constant (k1) as a function of reaction temperature for the decomposition of H_2O_2(0.5 mM; 50 ml) catalyzed by different oxides. CeO_2(red square), CuO (blue diamond), HfO_2(green triangle), Gd_2O_3(purple circle) and Fe2O3(blue stars). SA: Fe_2O_3(4.5 m2),CeO_2(7.5 m2); CuO (0.3 m2); HfO_2(7.5 m2); Gd_2O_3(1.7 m2).

Table 4. The activation energy (E_a), frequency factor (A), standard enthalpies of activation ($\Delta^{\ddagger}H^{\circ}$) and particle size for the decomposition of H_2O_2 for the oxides.

Material	E_a (kJ·mol^{-1})	A (s^{-1})	$\Delta^{\ddagger}H^{\circ}$ (kJ·mol^{-1})	Particle size
Fe_2O_3	47 ± 1	2.2×10^3	44 ± 1	< 5 μm
CeO_2	40 ± 1	1.4×10^3	37 ± 1	14 μm
CuO	76 ± 1	3.5×10^9	73 ± 1	< 50 nm
HfO_2	60 ± 1	1.1×10^7	57 ± 1	44 μm
Gd_2O_3	63 ± 1	3.4×10^6	60 ± 1	12 nm

3.1.2 Mechanistic studies

The $OH^{\cdot}$ radical has shown a high affinity for forming "bonded states" with exposed metal cations at the surface and in cases where the interaction is weak enough, it is possible that that $OH^{\cdot}$ radical can react with H_2O_2 and this will affect the types of products which form on the surface.
The decomposition of H_2O_2 at the surface will be followed by a formation of $OH^{\cdot}$ and this has been monitored on the oxides mentioned with the modified version of the Hantzsch method. Within this method, $OH^{\cdot}$ reacts with Tris buffer leading to the formation of formaldehyde, CH_2O which has the absorption wavelength of 368 nm and is detected with UV/vis spectroscopy. The correlation between the amount of CH_2O formed and the amount produced $OH^{\cdot}$ has been obtained and this will also be dependent of the relative reactivity of the adsorbed $OH^{\cdot}$ radicals.

The dynamics of the $OH^{\cdot}$ formation can thereby be viewed through the formation of CH_2O seen in Fig. 16, showing that there is a significant difference between the yields and curve shapes for the oxides. The highest formation of the $OH^{\cdot}$ can be seen for CuO, followed by Fe_2O_3 and then by CeO_2 and HfO_2.

The formation of CH_2O viewed as a function of H_2O_2 conversion for the earlier mentioned oxides together with oxides previously published from our group is seen in Fig. 17**.** The amount of CH_2O is dependent both on the amount of $OH^{\cdot}$ and on its reactivity. It can be seen that the release of CH_2O differs for the different materials.

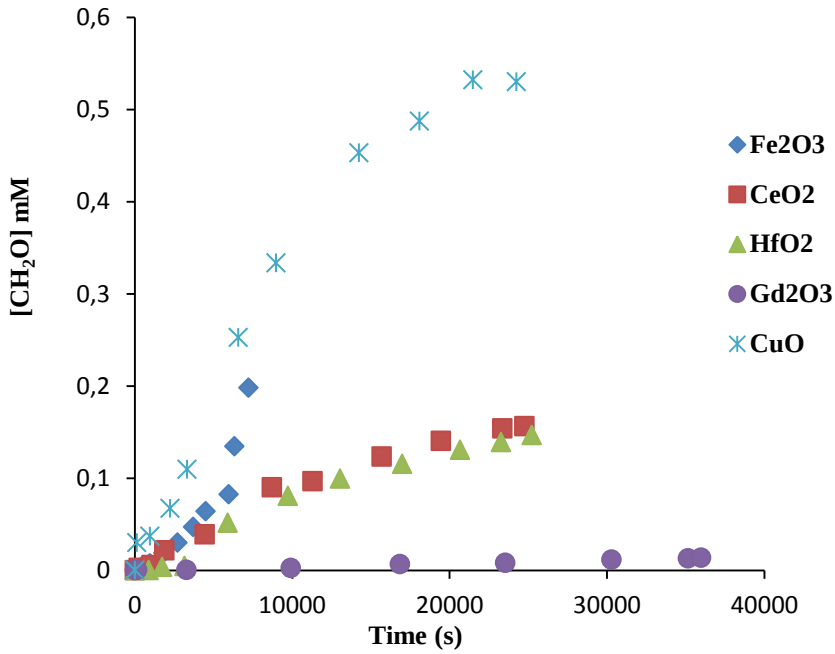

Figure 16. Formaldehyde formed by reaction of HO radicals with Tris during decompo-sition of H_2O_2(5 mM; 50 ml) catalyzed by different oxides: CeO_2(red square), CuO (blue stars), HfO_2(green triangle), Gd_2O_3(purple circle) and Fe_2O_3 (blue diamond).

The differences seen in the release behavior could be explained by a slow catalytic decomposition of H_2O_2 in comparison with the adsorption that would result in a low release in the initial stage. The $OH^{\cdot}$ release rate would only reach its maximum, after a full coverage of H_2O_2 on the surface. This behavior was seen for Gd_2O_3 and TiO_2, having a fast adsorption of H_2O_2 but a low $OH^{\cdot}$ release and no clear turnover point. It should be noted that a lower amount of Gd_2O_3 compared to the other oxides was used in the experiments due to the rapid catalytic decomposition of H_2O_2. The opposite behavior is seen for ZrO_2 with a high initial $OH^{\cdot}$ release, which could indicate a weak adsorption of H_2O_2 and a fast decomposition process.

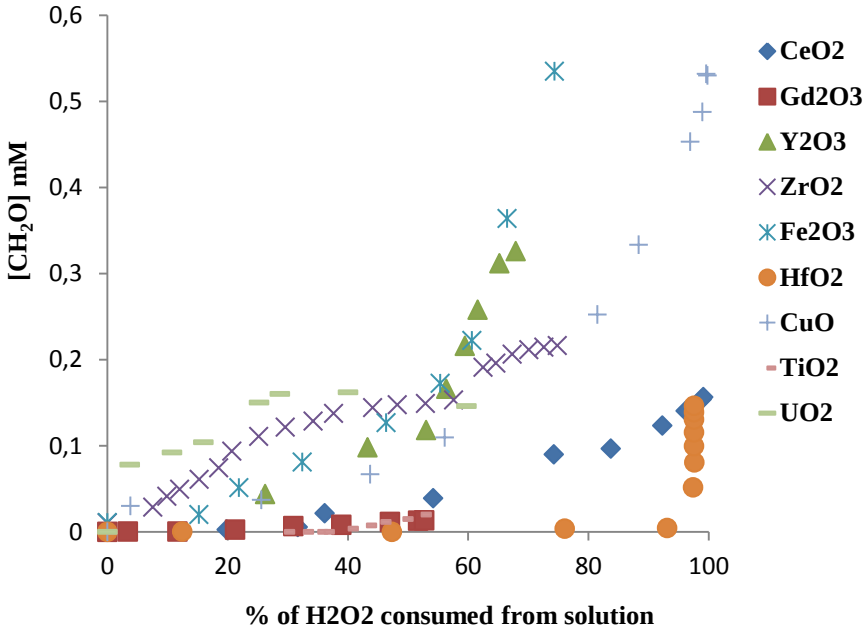

Figure 17. Amount of CH_2O present in the reaction system as a function of the percentage of H_2O_2 consumed from solution during reaction with different oxide materials: CeO_2(blue diamond); Gd_2O_3(red square); Y_2O_3(green triangle); ZrO_2(×); Fe_2O_3(blue stars); HfO_2(yellow circle); CuO (+); TiO_2(-); UO_2(−).

A turnover point can be seen for most oxides. This can be explained by the fact that the $OH^{\cdot}$ radical can react with both the Tris and the H_2O_2. The reaction with Tris is two orders of magnitude faster than with H_2O_2, and the presence of H_2O_2 will thereby have an influence on the CH_2O formation. The competition between them will thereby also be influenced by the relative surface coverage of H_2O_2. It should also be mentioned that they react differently with the surface due to differences in geometry and size. The interaction between H_2O_2 and the surface is much stronger than for Tris, due to both hydrogen bonding and the strong interaction between the cation and the oxygen in H_2O_2 [45]. The turnover point will depend on the H_2O_2 concentration when Tris starts to become the dominating reactant.

When interpreting the $OH^{\cdot}$ production it should be noted that it is not possible for the $OH^{\cdot}$ produced in redox reactions to scavenge with Tris, shown in [46]. This is of importance when explaining the $OH^{\cdot}$ release behavior for UO_2 where the formation of CH_2O reaches a plateau. This plateau corresponds to when the consumption of H_2O_2 has reached 20%. As mentioned earlier the H_2O_2 does not only undergo catalytic decomposition, it will also oxidize the surface and the oxidation product UO_2^{2+} is water soluble. The dissolution of the oxidation product will expose a fresh unoxidized surface.

DFT calculations have been performed by C. Lousada et al [19, 47] for the reaction of H_2O_2 with these oxide clusters and reactivity descriptors such as Ionization potential, Pauling electronegativity and Mulliken charge have been plotted towards Arrhenius activation energy and correlations been found.

A higher E_a was first seen to correspond to a lower adsorption energy for $OH^{\cdot}$, which was also shown to be inversely proportional to the Pauling electronegativity of the metal atom present, for transition metal oxides. The adsorption energy of the $OH^{\cdot}$ correlated to the energy barrier for the H_2O_2 decomposition, i.e. a strong adsorption would result in a lower energy barrier. The DFT ionization potential and Mulliken electronegativity of the metal cation were inversely proportional to the energy barrier for H_2O_2 decomposition and the activation energy.

The CuO has the highest E_a seen in Table 4 and shows the lowest ionization potential and Mulliken electronegativity as seen in [19] which is expected to result in a high energy barrier for the H_2O_2 decomposition and thereby in a less strong adsorption of the OH radical. This would also lead to a lower Lewis acidity making the OH bonds weaker and eventually resulting in a surface that is more available for accommodating H_2O_2. As seen in both Fig. 15 and 16,

this is true in the case of CuO, showing a higher release of $OH^{\cdot}$ radicals. Fe_2O_3 had almost as low ionization potential and Mulliken electronegativity and is also showing a high release of $OH^{\cdot}$.

TiO_2 has a low E_a which corresponded to a high ionization potential and Mulliken electronegativity resulting in a high Lewis acidity leading to a stronger bond with OH^- groups from the dissociative adsorption of H_2O, making the surface less available for the H_2O_2 accommodation. It can be seen in fig. 16 that the formation of $OH^{\cdot}$ is very low.

Al_2O_3 is also having a low E_a and should according to [48] have a high Lewis acidity, as is the case of Cr_2O_3. These properties should, as in the case of Ti, result in a low accommodation of H_2O_2 and also in a low formation of $OH^{\cdot}$.

The behavior of Al_2O_3 and Cr_2O_3 as dopants in UO_2 fuel pellets, i.e. ADOPT, is discussed in the next section.

3.2 Oxidative dissolution of ADOPT compared to standard UO_2 fuel

3.2.1 H_2O_2 induced dissolution of UO_2

The catalytic decomposition of H_2O_2 has been discussed. The difference from the earlier studied oxides and the UO_2 is the ability of the UO_2 to undergo dissolution as a consequence of the oxidation by H_2O_2. This will result in two possible reaction pathways; either the oxidative dissolution, releasing UO_2^{2+} into solution, or just the catalytic decomposition of H_2O_2 leaving the surface unchanged. Studying the dissolution yield for doped UO_2 pellets is one way to understand the mechanism.

The decomposition of H_2O_2 in contact with the two pellets and the resulting dissolution of U(VI) are represented for ADOPT and pure UO_2 pellets in Fig. 18 where the H_2O_2 concentration (right axis) and the U(VI) concentration (left axis) are plotted against reaction time**.**

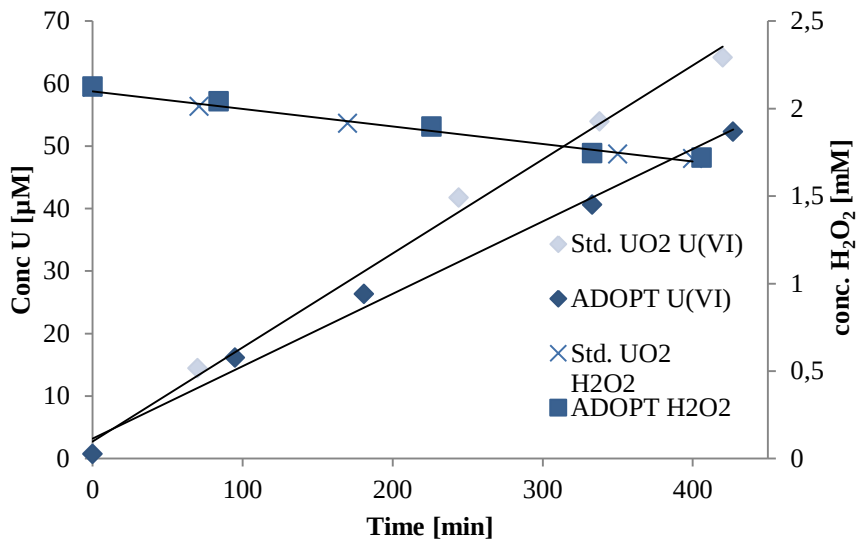

Figure 18, U(VI) concentration plotted versus time for std. UO_2 and ADOPT is on the left side and the decomposition of H_2O_2 is viewed on the right side.

This was done in order to find out if the reactivity towards H_2O_2 would change when a std. UO_2 is doped with oxides as in the case of the ADOPT fuel. ADOPT is as mentioned a UO_2 pellet doped with 1000 ppm of Cr_2O_3 and Al_2O_2 oxides which has shown to enhance the grain size, density and decrease the fission gas diffusion [6] and a smoother surface [27, 49].

As can be seen, no significant difference in the rate of H_2O_2 consumption can be observed for the two materials. This is in agreement with the results of previous studies on doped UO_2 compared to pure UO_2 [29, 32, 46]. However, a small but significant difference in uranium dissolution rate can be observed. For pure UO_2 the dissolution rate is $1.3 \pm 0.1 \times 10^{-7}$ mol m^{-2} s^{-1} while for ADOPT the corresponding value is $1.0 \pm 0.1 \times 10^{-7}$ mol m^{-2} s^{-1}. The rates for H_2O_2 consumption and uranium dissolution are summarized in Table 5.

Table 5. Reactions rates for H_2O_2 consumption and U(VI) dissolution for std. UO_2 and ADOPT Pellet under N_2 atmosphere

	Std. UO_2 mol/s, m^2	ADOPT mol/s, m^2
U(VI)	$1.3 \pm 0.1 \times 10^{-7}$	$1.0 \pm 0.1 \times 10^{-7}$
H_2O_2	$8.5 \pm 0.9 \times 10^{-7}$	$7.7 \pm 1 \times 10^{-7}$

The observed difference in dissolution yield could impose that aluminum or chromium oxides have the same effect on the redox reactivity of UO_2 as observed for other dopants. However, the effect is very small compared to previous studies. A direct comparison of the rates between the two materials could easily be misleading since there could be small differences in exposed surface area that are

impossible to control. Therefore, a comparison of the dissolution yields is more relevant as this cancels any differences in exposed surface area. The kinetic dissolution yield (i.e., the ratio between the rate of uranium dissolution and the rate of H_2O_2 consumption) in this study are 15 % for pure UO_2 and 12 % for ADOPT. This difference, considering the experimental uncertainty, is too small to be regarded as significant. These values are well in line with the previously reported dissolution yield for commercial UO_2 pellets [29]. Given the low concentrations of dopants in ADOPT, the insignificant difference is not completely unexpected.

3.2.2 Radiation induced dissolution of UO_2

The radiation induced dissolution of U(VI) from the two pellets are presented in table 6 and was obtained by measuring the U(VI) dissolution before and after irradiations.

All four pellets were irradiated together for 48 and 65 h, respectively, in different positions being exposed to different dose rates, measured by Fricke dosimetry [5] with total doses in the range between 15 000 and 37 000 Gy. The resulting uranium dissolution rates (based on 10 experiments per pellet) are summarized in Table 6.

Table 6. U(VI) release during γ irradiation in 10mM $NaHCO_3$ solution and under N_2 atm.

	Std.UO_2 mol/ Gy s^{-1}, m^2	ADOPT mol/ Gy s^{-1}, m^2
U(VI)	$1.8 \pm 0.1 \times 10^{-8}$	$1.4 \pm 0.1 \times 10^{-8}$

As can be seen, there is a small but significant difference in the rate of radiation induced dissolution of the two materials. The difference is of the same magnitude as the difference in absolute uranium dissolution rates in the H_2O_2 exposure experiments and could thus be attributed to a difference in the exposed surface area, if any. It is interesting to compare the trends found in this work with the trends observed in a similar study on SIMFUEL and UO_2. In the latter study, the difference in uranium dissolution upon exposure to H_2O_2 under the same conditions as in this work was much larger than the difference observed upon exposure to γ-radiation. In the case of SIMFUEL, this was attributed to reduced redox reactivity which was more strongly pronounced upon exposure to the fairly weak oxidant H_2O_2 compared to γ-radiolysis where significantly stronger oxidants are present [31]. If the effect of dopants in the ADOPT pellets would be to decrease the redox reactivity of the UO_2 matrix, we would expect a similar trend when comparing exposure to H_2O_2 and γ-radiation, i.e. the difference between ADOPT and UO_2 would be smaller in the γ-radiolysis experiment than in the H_2O_2 experiment.

The presence of aluminum and chromium in the leaching solutions was analyzed using ICP-OES but the concentrations were below the detection limit (0.5 ppm)

3.3 Leaching studies using spent fuel

There are both physical and chemical changes occurring in the UO_2 pellet during the in reactor use. All of these changes are not possible to replicate in a SIMFUEL, thereby its necessary to investigate the spent nuclear fuel.

The conditions for the leaching experiment of spent nuclear fuel, being performed in a Hot Cell at Studsvik, are not exactly the same as for the experiments performed with the fresh pellets at KTH. The solution also contains 10 mM NaCl and the concentration of $NaHCO_3$ is 2 mM instead of 10 mM. The solution has not been purged N_2, e.g. there will be a higher presence of O_2. Even though the conditions differ to a large extent, we are still comparing a std. UO_2 with an ADOPT fuel as before.

The cumulative release fractions (i.e., the amount of each nuclide in the leachant divided by the initial amount of the nuclide in the fuel sample, accumulated over all contact periods [9]) are presented in fig. 18. As can be seen, the ^{238}U release for the ADOPT is lower than for standard UO_2 fuel. However, the difference is fairly small and could simply be attributed to differences in exposed surface area.

One possible reason for a difference in exposed reactive surface area is the difference in grain size. Larger grain size implies lower density of grain boundaries per surface area and thereby lower reactivity. To further explore this possible difference, the release of other radionuclides relative to the uranium release can be compared. The results from the three first contact periods have been published previously [14, 15]. The cumulative release of the radionuclides after a total contact time of 360 days can be found in Table 8. The elements are divided according to UO_2 matrix solubility. To allow a more accurate comparison between ADOPT and conventional UO_2

fuel, the cumulative release fraction of the radionuclides relative to the cumulative release fraction of ^{238}U is also given in Table 7.

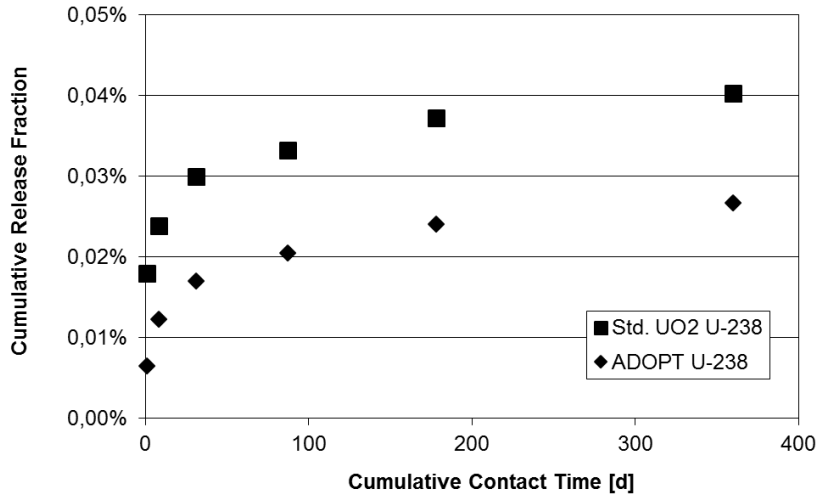

Figure 19. Cumulative release fractions as a function of the cumulative contact time [days].

The table shows a slightly higher release of lanthanides and actinides relative to the matrix for the conventional UO_2. However, the observed difference is relatively small. It should also be mentioned that the concentrations of lanthanides found in the leaching solutions (and consequently also the calculated release fractions) are relative low. This can partly be attributed to sorption of lanthanides on to the walls of the leaching vessels [9].

However, the release of fission products with low UO_2 solubility display some interesting differences. The most apparent difference is that the fraction of Cs released during the experiments is much higher for conventional UO_2 fuel than for ADOPT fuel. For the other elements of low UO_2 solubility the trend is the opposite, i.e., a higher fraction is dissolved for ADOPT than for conventional UO_2 fuel. As Cs is one of the main elements contributing to the instant release fraction, it is not unexpected that ADOPT releases a lower fraction

given the fact that the grain size is larger for ADOPT, i.e., the diffusion distance to the surface is longer. Interestingly, the relative cumulative release fraction for the elements with low UO_2 solubility for the last contact period shown in Table 8 displays a consistent difference between ADOPT and standard UO_2.

Interestingly, the relative cumulative release fraction for the elements with low UO_2 solubility for the last contact period displays a consistent difference between ADOPT and standard UO_2 according to Table 7. As can be seen, the relative release is higher for ADOPT than for the standard UO_2 fuel. For Cs it is clear that the initial contact period displays the opposite trend, i.e., a higher relative release for standard UO_2 compared to ADOPT. While the difference in initial Cs release can most probably be attributed to the difference in grain size and thereby diffusion distance, the difference observed for the other elements can be attributed to differences in matrix solubility. As the dopants in ADOPT will reduce the hyperstochiometry of the matrix, the fission product solubility will be less soluble as reflected by the significantly higher release fraction.

Table 7. Relative cumulative release fraction for the last contact period

	Std. UO_2	ADOPT
^{100}Mo	40	83
^{90}Sr	1.2	1.6
^{99}Tc	24	49
^{137}Cs	85	118
^{138}Ba	0.06	0.01
^{85}Rb	18	25
^{238}U	1	1

Table 8. The cumulative release after total contact time of 360 days.

	Std.UO_2 [a]	ADOPT[a]	Std.UO_2 [b]	ADOPT[b]
Low UO_2 solubility				
^{137}Cs	1.57×10^{-2}	9.69×10^{-3}	3894%	3627%
^{99}Tc	2.08×10^{-3}	3.01×10^{-3}	516%	1127%
^{100}Mo	4.29×10^{-3}	5.55×10^{-3}	1064%	2079%
^{90}Sr	9.88×10^{-4}	7.36×10^{-4}	245%	276%
^{138}Ba	4.62×10^{-4}	3.21×10^{-4}	115 %	120%
^{85}Rb	3.16×10^{-3}	3.01×10^{-3}	785%	1128 %
UO_2 matrix:				
Lanthanides				
^{139}La	1.23×10^{-4}	3.15×10^{-5}	30%	12%
^{140}Ce	1.23×10^{-4}	3.35×10^{-5}	31%	13%
^{141}Pr	1.29×10^{-4}	3.19×10^{-5}	32%	12%
^{144}Nd	1.21×10^{-4}	3.06×10^{-5}	30%	11%
^{153}Eu	1.22×10^{-4}	3.10×10^{-5}	30%	12%
Actinides				
^{238}U	4.03×10^{-4}	2.67×10^{-4}	100%	100%
^{237}Np	3.63×10^{-4}	2.45×10^{-4}	90%	92%
^{239}Pu	1.59×10^{-4}	5.96×10^{-5}	39%	22%
^{244}Cm	1.51×10^{-4}	3.29×10^{-5}	37%	12%

a) The cumulative release after total contact time of 360 days.
b) The release of each nuclide compared to ^{238}U in percent.

4. Conclusions

Regarding the catalytic decomposition of H_2O_2 on oxides:

- A kinetic study including first and second order rate constants together with Arrhenius parameters for decomposition of H_2O_2, by oxides like Gd_2O_3, HfO_2, CeO_2, Fe_2O_3 and CuO was performed experimentally. It could be concluded that the reactivity of H_2O_2 towards these oxides differs significantly in spite of the similarities between them
- A mechanistic study where the yields and dynamics of the formation of the intermediate $HO^{\cdot}$ radical from the decomposition of H_2O_2 were determined for the oxides and seen to differ considerably between the oxides.
- A turnover point could be found for all oxides studied, showing an increased amount of scavenged $HO^{\cdot}$ radical after different amount consumed H_2O_2 for the different oxides.

Regarding the oxidative dissolution of UO_2 and ADOPT:

- The reactivity of the std. UO_2 and ADOPT towards H_2O_2 was as in agreement with previous studies.
- The difference in oxidative dissolution from the radiation exposure was small but significant. These results are more likely attributed to a difference in exposed surface area than an effect in

doping. The insignificant difference in oxidative dissolution yield is supporting the same conclusion.

- The leaching experiments performed on irradiated fuel show a similar behavior with a small difference in ^{238}U release, also being explained by differences in surface area.
- The release of lanthanides and actinides is slightly lower relative to the matrix for ADOPT, however the difference is relatively small.
- The release of fission products with low UO_2 solubility show a higher release from ADOPT due to different matrix solubility. The release of Cs is on the other hand larger from std. UO_2 which is attributed to the larger grain size of ADOPT, extending the diffusion distance.

5. Acknowledgements

I would firstly like to thank my supervisor Mats Jonsson for your support, patience and scientific guidance. Secondly I would want to thank my second supervisor Olivia Roth for your time and for always being honest with me. I would also really want to thank:

Inna Soroka, for your support, our talks and our chocolate moments in the office.

Beatrice Johansson, for being my first and only diploma worker, for always bringing me nice coffee. And for continuing being my friend.

Sara Skoglund, for the company in the lab, our coffee breaks and for always being you. And thanks for your smile =)

Anton, Boris, Constantin and Dimitri for never making me feel lonely in the lab, for being calm and not so active ;)

My colleagues at the former group of nuclear chemistry; Inna, Karin, Cláudio, Veronica, Alex, Yang, Susanna, Mats Jansson, and Åsa for sharing your knowledge. Johan and Gabor for being you and for giving me an idée of how it could had been to study at KTH. Once again thank you Inna and Karin for reading and giving valuable comments on this thesis.

My friends at physical chemistry group for adding me to your cake email list ;) for the moments when my ability to smell the cake couldn´t be trusted… and for always treating me as one of you.

I am also very thankful for the help and support from the staff at Studsvik, especially Johan Söderberg for the nice company while looking after me in the Hot Cell lab.

The Swedish Nuclear Fuel and Waste Management Co, SKB, is gratefully acknowledged for financial support.

Finally I would like to thank my family and friends for being in my life =)

6. References

[1] A. vid, K.o.U.A. (KSU), Kärnkraften i vår omvärld, in, 2008.

[2] L. F. Auqué, M. J. Gimeno, J. B. Gómez, I. Puigdomenech, J. A. T. Smellie, E-L. Tullborg, Groundwater chemistry around a repository for spent nuclear fuel over a glacial cycle. Evaluation for SR-Can, in, 2006.

[3] skb.se.

[4] SKB, TR-10-12 Design and production of the KBS-3 repository, in, Swedish Nuclear Fuel and Waste Management Co, www.skb.se, 2010.

[5] G. Choppin, J.O. Liljenzin, J. Rydberg, Radiochemistry and Nuclear Chemistry, Reed Educational and Professional Publishing Ltd, Oxford, 1995.

[6] J. Arborelius, K. Backman, L. Hallstadius, M. Limbaeck, J. Nilsson, B. Rebensdorff, G. Zhou, K. Kitano, R. Loefstroem, G. Roennberg, Advanced doped UO2 pellets in LWR applications, J. Nucl. Sci. Technol., 43 (2006) 967-976.

[7] C. Degueldre, J. Bertsch, G. Kuri, M. Martin, Nuclear fuel in generation II and III reactors: research issues related to high burn-up, Energy Environ. Sci., 4 (2011) 1651-1661.

[8] L. Johnson, I. Guenther-Leopold, J. Kobler Waldis, H. P. Linder, J. Low, D. Cui, E. Ekeroth, K. Spahiu, L. Z. Evins, Rapid aqueous release of fission products from high burn-up LWR fuel: Experimental results and correlations with fission gas release, J. Nucl. Mater., 420 (2012) 54-62.

[9] U. Zwicky, J. Low, E. Ekeroth, TR-11-03, Corrosion Studies with High Burnup Light Water Reactor Fuel, in, SKB Svensk Kärnbränslehantering AB, Stockholm, Sweden, 2011, 2003.

[10] H. Matzke, Radiation damage-enhanced dissolution of UO2 in water, J. Nucl. Mater., 190 (1992) 101-106.

[11] O. Roth, S. Nilsson, M. Jonsson, Radiation enhanced reactivity of UO2, J. Nucl. Mater., 354 (2006) 131-136.

[12] D. W. Shoesmith, Fuel corrosion processes under waste disposal conditions, J. Nucl. Mater., 282 (2000) 1-31.

[13] T. E. Eriksen, D. W. Shoesmith, M. Jonsson, Radiation induced dissolution of UO2 based nuclear fuel - A critical review of predictive modelling approaches, J. Nucl. Mater., 420 (2012) 409-423.

[14] O. Roth, J. Low, M. Granfors, K. Spahiu, Effects of matrix composition on instant release fractions from high burn-up nuclear fuel, Mater. Res. Soc. Symp. Proc., Vol. 1518 (2013).

[15] O. Roth, J. Low, K. Spahiu, Effects of matrix composition and sample preparation on instant release fractions from high burnup nuclear fuel (Article not jet accepted).

[16] I. Grenthe, D. Ferri, F. Salvatore, G. Riccio, Studies on metal carbonate equilibria. Part 10. A solubility study of the complex formation in the uranium(VI)-water-carbon dioxide (g) system at 25 [degree]C, J. Chem. Soc. Dalton Trans., (1984) 2439-2443.

[17] J. A.T. Smellie, M. Laaksoharju, P. Wikberg, Äspö, SE Sweden: a natural groundwater flow model derived from hydrogeochemical observations, J. Hydrol., 172 (1995) 147-169.

[18] S. Le Caer, Water Radiolysis: Influence of Oxide Surfaces on H-2 Production under Ionizing Radiation, Water, 3 (2011) 235-253.

[19] C. M. Lousada, Reactions of aqueous radiolysis products with oxide surfaces: An experimental and DFT study, in, KTH, 2013.

[20] J.R.A. Godinho, S. Piazolo, L.Z. Evins, Effect of surface orientation on dissolution rates and topography of CaF2, Geochimica et Cosmochimica Acta, 86 (2012) 392-403.

[21] A. Mayoral, H. Barron, R. Estrada-Salas, A. Vazquez-Duran, M. Jose-Yacaman, Nanoparticle stability from the nano to the meso interval, in: The Royal Society of Chemistry, 2009, pp. 8.

[22] K. W. Song, Y. H. Jeong, K. S. Kim, J. G. Bang, T. H. Chun, H. K. Kim, K. N. Song, High burnup fuel technology in Korea, Nucl. Engin. Technol., 40 (2008) 21-36.

[23] A. Leenaers, L. de Tollenaere, C. Delafoy, S. Van den Berghe, On the solubility of chromium sesquioxide in uranium dioxide fuel, J. Nucl. Mater., 317 (2003) 62-68.

[24] S. C. Middleburgh, R. W. Grimes, K. H. Desai, P. R. Blair, L. Hallstadius, K. Backman, P. Van Uffelen, Swelling due to fission products and additives dissolved within the uranium dioxide lattice, J. Nucl. Mater., 427 (2012) 359-363.

[25] S. C. Middleburgh, D. C. Parfitt, R. W. Grimes, B. Dorado, M. Bertolus, P. R. Blair, L. Hallstadius, K. Backman, Solution of trivalent cations into uranium dioxide, J. Nucl. Mater., 420 (2012) 258-261.

[26] M. W. D. Cooper, D. J. Gregg, Y. Zhang, G. J. Thorogood, G. R. Lumpkin, R. W. Grimes, S. C. Middleburgh, Formation of $(Cr,Al)UO_4$ from doped UO_2 and its influence on partition of soluble fission products, J. Nucl. Mater., 443 (2013) 236-241.

[27] K. D. O'Neil, H. He, P. Keech, D. W. Shoesmith, O. A. Semenikhin, Anisotropy of local electrical conductivity of hyper-stoichiometric uranium dioxide revealed by current-sensing atomic force microscopy (CS-AFM), Electrochem. Commun., 10 (2008) 1805-1808.

[28] M. Jonsson, E. Ekeroth, O. Roth, Dissolution of UO2 by one- and two-electron oxidants, in: V.M. Oversby, L.O. Werme (Eds.) Scientific Basis for Nuclear Waste Management Xxvii, 2004, pp. 77-82.

[29] R. Pehrman, M. Trummer, C. M. Lousada, M. Jonsson, On the redox reactivity of doped UO2 pellets - Influence of dopants on the H2O2 decomposition mechanism, J. Nucl. Mater., 430 (2012) 6-11.

[30] M. Jonsson, F. Nielsen, O. Roth, E. Ekeroth, S. Nilsson, M. M. Hossain, Radiation induced spent nuclear fuel dissolution under deep repository conditions, Environmental Science & Technology, 41 (2007) 7087-7093.

[31] E. Ekeroth, O. Roth, M. Jonsson, The relative impact of radiolysis products in radiation induced oxidative dissolution of UO2, J. Nucl. Mater., 355 (2006) 38-46.

[32] S. Nilsson, M. Jonsson, H2O2 and radiation induced dissolution of UO2 and SIMFUEL pellets, J. Nucl. Mater., 410 (2011) 89-93.

[33] E. Ekeroth, M. Jonsson, Oxidation of UO2 by radiolytic oxidants, J. Nucl. Mater., 322 (2003) 7.

[34] M. M. Hossain, E. Ekeroth, M. Jonsson, Effects of HCO3- on the kinetics of UO2 oxidation by H2O2, J. Nucl. Mater., 358 (2006) 202-208.

[35] C. M. Lousada, M. Jonsson, Kinetics, Mechanism, and Activation Energy of H2O2 Decomposition on the Surface of ZrO2, J. Phys. Chem. C, 114 (2010) 11202-11208.

[36] M. Trummer, B. Dahlgren, M. Jonsson, The effect of Y2O3 on the dynamics of oxidative dissolution of UO2, J. Nucl. Mater., 407 (2010) 195-199.

[37] M. Trummer, S. Nilsson, M. Jonsson, On the effects of fission product noble metal inclusions on the kinetics of radiation induced dissolution of spent nuclear fuel, J. Nucl. Mater., 378 (2008) 55-59.

[38] C. M. Lousada, A. J. Johansson, T. Brinck, M. Jonsson, Reactivity of metal oxide clusters with hydrogen peroxide and water - a DFT study evaluating the performance of different exchange-correlation functionals, Phys. Chem. Chem. Phys., 15 (2013) 5539-5552.

[39] M. Trummer, M. Jonsson, Resolving the H2 effect on radiation induced dissolution of UO2-based spent nuclear fuel, J. Nucl. Mater., 396 (2010) 163-169.

[40] Z. Szabo, H. Moll, I. Grenthe, Structure and dynamics in the complex ion (UO2)2(CO3)(OH)3, J. Chem. Soc. Dalton Trans., (2000) 3158-3161.

[41] S.B. Savvin, Analytical applications of Arsenazo III-III* The mechanism of complex formation between III and certain elements, Pergamon Press Ltd., Vol. 11 (1963) pp. 7 to 19.

[42] W.A. Patrick, H.B. Wagner, Determination of hydrogen peroxide in small concentrations. A spectrophotometric method. , Anal. Chem, 21 (1949) 1279-1280

[43] C. M. Lousada, M. Yang, K. Nilsson, M. Jonsson, Catalytic decomposition of hydrogen peroxide on transition metal and lanthanide oxides, J. Mol. Catal. A: Chem., 379 (2013) 178-184.

[44] G.E. Brown, V.E. Henrich, W.H. Casey, D.L. Clark, C. Eggleston, A. Felmy, D.W. Goodman, M. Grätzel, G. Maciel, M.I. McCarthy, K.H. Nealson, D.A. Sverjensky, M.F. Toney, J.M. Zachara, Metal Oxide Surfaces and Their Interactions with Aqueous Solutions and Microbial Organisms, Chemical Reviews, 99 (1998) 77-174.

[45] C. M. Lousada, A. J. Johansson, T. Brinck, M. Jonsson, Mechanism of H2O2 Decomposition on Transition Metal Oxide Surfaces, J. Phys. Chem. C, 116 (2012) 9533-9543.

[46] C. M. Lousada, M. Trummer, M. Jonsson, Reactivity of H2O2 towards different UO2-based materials: The relative impact of radiolysis products revisited, J. Nucl. Mater., 434 (2013) 434-439.

[47] C. M Lousada, T. Brinck, M. Jonsson, Application of reactivity descriptors to the catalytic decomposition of hydrogen peroxide at oxide surfaces, Chem. European J., under review, (2013).

[48] V.E. Henrich, P.A. Cox, The Surface Science of Metal Oxides, 1994.

[49] T. Matsui, K. Naito, Electrical-conductivity measurement and thermogravimetric study of chromium-doped uranium-dioxide, J. Nucl. Mater., 137 (1986) 212-216.